Quantum Chaos

H. J. Korsch and H. Wiescher

Fachbereich Physik, Universität Kaiserslautern, D-67653 Kaiserslautern, Germany,
e-mail: korsch@physik.uni-kl.de

Abstract. The study of dynamical quantum systems, which are classically chaotic, and the search for quantum manifestations of classical chaos, require large scale numerical computations. Special numerical techniques developed and applied in such studies are discussed: The numerical solution of the time-dependent Schrödinger equation, the construction of quantum phase space densities, quantum dynamics in phase space, the use of phase space entropies for characterizing localization phenomena, etc. As an illustration, the dynamics of a driven one-dimensional anharmonic oscillator is studied, both classically and quantum mechanically. In addition, spectral properties and chaotic tunneling are addressed.

1 Classical and Quantum Chaos

During the last three decades it has become evident that the dynamics of simple Hamiltonian systems can be remarkably complex. Typical examples of such 'simple' systems are a point mass in a two-dimensional time-independent potential, or — even simpler — an explicitly time-dependent system with a single degree of freedom. In many important cases, such a system can be considered as time-periodic. The best studied case is certainly the celebrated forced or parametrically excited harmonic oscillator. Numerous papers have been published, which analyze the classical or quantum dynamics of such a harmonic oscillator in much detail. One should be aware of the fact, however, that the harmonic oscillator is a very special case: The classical equations of motion are linear. For all other systems this is not the case. Their behavior is the studied in 'non-linear dynamics'.

It is well-known that deterministic classical systems show erratic, irregular behavior. Moreover, this chaotic dynamics is a generic property: Typical systems show an intricate mixture of regular and irregular motion, whose structural organization can be most conveniently displayed by means of Poincaré sections of phase space. Rather than analyzing a full trajectory in the higher-dimensional phase space, one considers only its intersections with a reasonably chosen surface. In this way, the dynamics can be treated as a discrete mapping.

Such a discretization is of particular simplicity for time-periodic systems with one degree of freedom: Here one can look at the system stroboscopically, i.e. at times $t_n = nT$, $n = 0, 1, \ldots$, where T is the period. Figure 1 shows such a phase space plot for a forced non-harmonic oscillator (see Sect. 4 for details). Shown is a synoptic plot of several trajectories with different initial conditions. One observes regular regions, where the phase space points generated by a trajectory trace out

lines, the so-called invariant curves. Here the motion is regular. In addition, we find points, which cover an area in phase space. In fact, all these points in Fig. 1 are computed from a *single* trajectory, a chaotic one. Classically, a chaotic trajectory – or more generally chaotic dynamics – is defined by an exponential separation of initially nearby trajectories in the long time limit (more precisely a positive Lyapunov exponent). Numerical studies ('computer experiments') of this type are very helpful for studying chaotic dynamics and PC programs are available for many systems of interest in physics (Korsch and Jodl 1994). More details on the theory of the dynamics of Hamiltonian systems in context with quantum dynamics can be found in textbooks (see, e.g., Tabor (1989), Ozorio de Almeida (1988), Gutzwiller (1990)).

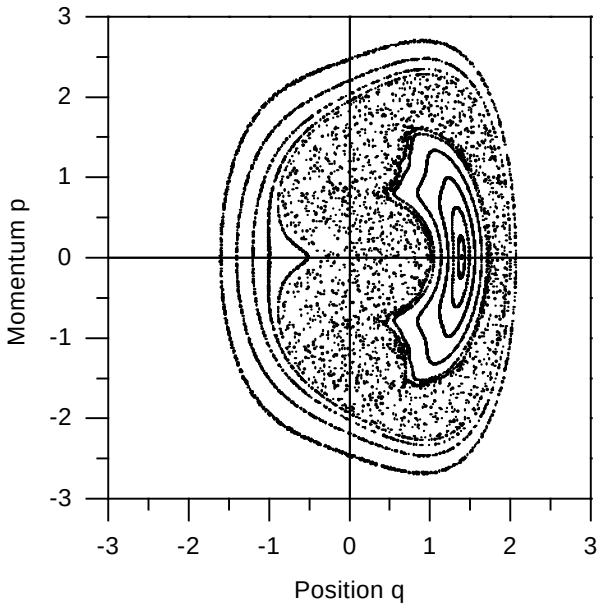

Fig. 1. Stroboscopic Poincaré section for a classical driven anharmonic oscillator.

Quantum dynamics, however, is governed by the Schrödinger equation

$$\mathrm{i}\hbar\,\dot{\psi} = H\,\psi \quad , \tag{1}$$

which is a *linear* equation, and it is therefore questionable if such a time evolution can be chaotic. For example, it is straightforward to show that – for a finite (N) dimensional Hilbert space – the time-dependent coefficients in a basis set expansion $\psi(t) = \sum_n c_n(t)\phi_n$ satisfy a finite system of coupled linear equations. Moreover, by separating real and imaginary parts, e.g. $c_n = q_n + \mathrm{i}p_n$, these

differential equations can be written as the canonical equations of motion of a classical N-dimensional harmonic oscillator, which is certainly *not* chaotic.

Nevertheless, classical mechanics is the limit of quantum mechanics for $\hbar \to 0$, and therefore it is of fundamental importance to understand this highly non-trivial limit, and considerable work has been done. This fascinating field of contemporary research is denoted as *'quantum chaos'* (Gutzwiller 1992) or *'post-modern quantum mechanics'* (Heller and Tomsovic 1993) and various excellent books by Gutzwiller (1990), Reichl (1992), Haake (1992), Feng and Yuan (1992), Nakamura (1993), as well as recent conference proceedings (Cvitanović et al. 1992, Gay 1992, Casati et al. 1993, Ikeda 1994) summarize the results.

In order to find the quantum manifestations (if any) of classical chaos, much of the recent research is supported by large scale computations (for small $\hbar$ the dimension of the Hilbert space is large, the wave functions are highly oscillatory, a long time propagation is of interest, etc) and special techniques for analyzing the system's behavior have been developed. Here, we will discuss some of these methods and illustrate their application to the seemingly simple case of time-periodic systems with one degree of freedom (see Casati and Molinari (1989) for an overview of the properties of such systems).

2 Quantum Time Evolution

The time evolution of a quantum state ψ is determined by the Schrödinger equation (1), which can be solved numerically by numerous methods. Among the most popular and efficient ones is an expansion in a discrete basis set, which converts the Schrödinger equation into a set of coupled linear differential equations, and – with an increasing number of applications – the direct solution as a partial differential equation in the coordinate representation, e.g.

$$\mathrm{i}\hbar \, \frac{\partial \psi(\mathbf{x},t)}{\partial t} = H\psi(\mathbf{x},t) = \left(-\frac{\hbar^2}{2m} \nabla^2 + V(\mathbf{x},t) \right) \psi(\mathbf{x},t) \ . \tag{2}$$

In addition, also a mixed treatment is possible (and sometimes also the most efficient strategy), where some of the degrees of freedom are treated by a basis set expansion and the remaining ones by solving a set of coupled differential equations.

One of the most powerful techniques for solving equation (2) is the so-called split-operator method (Feit et al. 1982), where the time propagator U for the Hamiltonian – splitted into a kinetic and potential energy part –

$$H\psi = \left(\frac{\mathbf{p}^2}{2m} + V(\mathbf{x}) \right) \psi = (K+V)\,\psi \tag{3}$$

can be approximated for a (small) time-step δ by

$$U(\delta) = \mathrm{e}^{-\frac{\mathrm{i}}{\hbar} H \delta} \approx \mathrm{e}^{-\frac{\mathrm{i}}{2\hbar} K \delta} \mathrm{e}^{-\frac{\mathrm{i}}{\hbar} V \delta} \mathrm{e}^{-\frac{\mathrm{i}}{2\hbar} K \delta} \ . \tag{4}$$

Observing now that the operator V is diagonal in the coordinate representation (i.e. a simple multiplication by the number $V(\mathbf{x})$), whereas the operator K is diagonal in the momentum representation (i.e. a multiplication by the number $\mathbf{p}^2/2m$), the time-propagation can be easily carried out by switching between the two representations by means of a Fast-Fourier-Transform (Press et al. 1986).

Different propagations schemes have been developed; for a critical comparison see Leforestier et al. (1991). Some more recent techniques are the staggered-time algorithm (Visscher 1991), the (unitary) forth oder method developed by De Raedt and Michielsen (1994), a multi-grid method (Becker et al. 1996), and the (t,t')-method (Peskin and Moiseyev 1993) based on an extended phase space description for explicitly time-dependent systems.

Here we will restrict ourselves to one degree of freedom, i.e. the numerical solution of

$$\mathrm{i}\hbar\,\frac{\partial\psi(x,t)}{\partial t} = -\frac{\hbar^2}{2m}\frac{\partial^2\psi(x,t)}{\partial x^2} + V(x,t)\psi(x,t) \tag{5}$$

with boundary conditions $\psi(x_{\min},t) = \psi(x_{\max},t) = 0$. We describe in some detail a numerical method, the so-called Goldberg algorithm (Goldberg 1967), (Koonin 1986), which works very well in this case.

First we discretize the coordinate x and construct the solution ψ_j only at points $x_j = x_{\min} + j\epsilon$, for $j = 1,\ldots,j_{\max}$ and $x_{j\max} = x_{\max}$.

Using a discrete expression for the second derivative

$$\left(\frac{\partial^2\psi}{\partial x^2}\right)_j = \frac{1}{\varepsilon^2}[\psi_{j+1} - 2\psi_j + \psi_{j-1}] + O(\varepsilon^2)\ , \tag{6}$$

the action of the Hamiltonian is given by

$$H\psi_j = -\frac{\hbar^2}{2m\varepsilon^2}[\psi_{j+1} - 2\psi_j + \psi_{j-1}] + V_j\psi_j\ . \tag{7}$$

Discretizing the time in equidistant steps δ, i.e. $t_n = t_0 + n\delta$, the wavefunction ψ_{n+1} at time t_{n+1} is obtained from ψ_n by

$$\psi_j^{n+1} = e^{-\frac{\mathrm{i}}{\hbar}H\delta}\,\psi_j^n\ . \tag{8}$$

Here it is *not* possible to approximate the exponential operator by $1 - \mathrm{i}H\delta/\hbar$, because such a non-unitary approximation leads to instabilities of the time-evolution. A uniform approximation is given by the Cayley form

$$\mathrm{e}^{-\frac{\mathrm{i}}{\hbar}H\delta} = \frac{1 - \frac{\mathrm{i}}{2\hbar}H\delta}{1 + \frac{\mathrm{i}}{2\hbar}H\delta} + O(\delta^3)\ , \tag{9}$$

which is correct up to second order in δ. Inserting now (9) into (8) and moving the denominator of (9) to the left hand side in (8), we obtain the iteration scheme

$$\psi_{j+1}^{n+1} + (\mathrm{i}\lambda - v_j^n - 2)\psi_j^{n+1} + \psi_{j-1}^{n+1} = -\psi_{j+1}^n + (\mathrm{i}\lambda + v_j^n + 2)\psi_j^n - \psi_{j-1}^n \tag{10}$$

with $\lambda = 4m\epsilon^2/\hbar\delta$ and $v_j^n = 2m\varepsilon^2 V(x_j, t_n)/\hbar^2$. These difference equations are stable and unitary, however implicit. The solution of the tridiagonal matrix equation (10) is a standard problem of numerical mathematics, which is solved by recursion (Goldberg 1967), (Koonin 1986) using the boundary conditions $\psi_0^n = \psi_{j_{\max}}^n = 0$. This method can be easily implemented numerically and allows a fast real-time solution of the Schrödinger equation on a PC. For the time-independent case, PC programs with graphical representation are available (Becker et al. 1988) and can be used for illustrating phenomena of elementary quantum mechanics, e.g. motion of wavepackets in various potentials, dynamics of coherent and squeezed harmonic oscillator states, tunneling through potential barriers, etc.

A few remarks on a reasonable choice of the parameters will be helpful. First, the mesh width ϵ determines the smallest wavelength, which can be accurately described on a discrete grid. A typical choice is $\epsilon = \hbar/5p_{\max}$, where $p_{\max}$ is the largest classical momentum. A reasonable choice of the time step is $\delta = m\epsilon^2/\hbar$, leading to a balance of the errors induced by time and space discretization (see (Goldberg 1967), (Koonin 1986), (Press et al. 1986) for more details).

It should be noted that a direct extension of the Goldberg algorithm to systems with more degrees of freedom requires a matrix inversion at each time step (the solution by recursion is no longer possible) and is therefore inefficient. Special techniques have been developed, however, which reduce the problem to intertwined one-dimensional ones; for details see (Schneider 1987), (Schneider and Wolter 1988, 1991).

3 Quantum State Tomography

3.1 Phase Space Distributions

In classical dynamics, the equations of motion (or experimental measurements) yield the trajectory $q(t)$ of the system for given initial conditions. This trajectory contains all information, but important dynamical features are only visible, if they are carefully extracted, e.g. by plotting the trajectory in adequate variables. Typically, one analyzes the dynamics in phase space (p, q), where the momentum $p(t)$ can be obtained from $q(t)$ by differentiation. In addition, one can restrict oneself to a section of phase space, the Poincaré section, as, e.g., the stroboscopic plot shown in Fig. 1 for a driven anharmonic oscillator. Such a plot reveals the dynamical properties of the system for all initial conditions and it provides a *global* description of the dynamical features of the system.

In quantum mechanics the situation is similar. As described above, one can numerically generate the wavefunction $\psi(x,t)$ in coordinate space as a function of time, but the essential dynamical features are still to be determined. The absolute square $|\psi(x,t)|^2$ yields the probability to find the particle at a given position, and by means of a Fourier transform of $\psi(x,t)$ to momentum space one obtains the overall probability for the momentum. In order to obtain information

about the momentum distribution at a given position, one can use the Gabor (or Fourier window) transformation

$$\langle p,q|\psi\rangle = \sqrt[4]{\frac{s}{\pi\hbar}} \int \exp\left[\frac{-s(x-q)^2}{2\hbar} - \mathrm{i}\,\frac{p}{\hbar}\left(x-\frac{q}{2}\right)\right] \psi(x)\,\mathrm{d}x \ . \tag{11}$$

This is a Fourier transform to momentum (p) space, which is weighted by a Gaussian window centered at position q. The so-called squeezing parameter s controls the width of the window. Up to a multiplicative factor, $\langle p,q|\psi\rangle$ is equal to the momentum distribution for $s = 0$, and the coordinate representation is reproduced for large s. Equation (11) can also be expressed as a projection of the wavefunction onto a so-called minimum uncertainty wavepacket (also called a coherent state):

$$\phi_{p,q}(x) = \sqrt[4]{\frac{s}{\pi\hbar}} \exp\left[\frac{-s(x-q)^2}{2\hbar} + \mathrm{i}\,\frac{p}{\hbar}\left(x-\frac{q}{2}\right)\right] \ , \tag{12}$$

a state with mean values q and p for position and momentum, respectively, and the uncertainties $\Delta p = \sqrt{\hbar s/2}$, $\Delta q = \sqrt{\hbar/2s}$, $\Delta p\,\Delta q = \hbar/2$. The squeezing parameter $s = \Delta p/\Delta q$ determines the ratio of the uncertainties and can be adapted to the problem under investigation. The absolute square

$$\rho_{\mathrm{H}}(p,q) = |\langle p,q|\psi\rangle|^2 = \left|\int \phi^*_{p,q}(x)\psi(x)\,\mathrm{d}x\right|^2 \tag{13}$$

with normalization

$$\frac{1}{2\pi\hbar}\int \rho_{\mathrm{H}}(p,q)\,\mathrm{d}p\,\mathrm{d}q = 1 \tag{14}$$

is called the Husimi density (Husimi 1940). It provides a quantum mechanical (quasi) probability distribution in phase space for a given wavefunction ψ and is very useful in an analysis of the classical – quantum correspondence in dynamical systems (Takahashi 1989).

3.2 Phase Space Entropy

The overall degree of localization in phase space can be obtained from the average information content measured by the phase space entropy

$$S = -\frac{1}{2\pi\hbar}\int \rho_{\mathrm{H}}(p,q)\,\ln\rho_{\mathrm{H}}(p,q)\,\mathrm{d}p\,\mathrm{d}q \ . \tag{15}$$

This entropy satisfies the inequality $S \geq 1$ (Wehrl 1978), which corresponds to the uncertainty relation $\Delta p\,\Delta q \geq \hbar/2$. The quantity e^S measures the number of minimum uncertainty states populated by the wavepacket and $A = 2\pi\hbar\,\mathrm{e}^S$ is the space area covered by the phase space distribution. It is instructive to calculate the entropy of a minimum uncertainty wavepacket (12) with squeezing

parameter s_0 analyzed by minimum uncertainty states with squeezing s_1. The result is simply

$$S = 1 + \ln \frac{s_0 + s_1}{2\sqrt{s_0 s_1}} \ . \tag{16}$$

Note that for $s_0 = s_1$ one obtains the smallest possible entropy $S = 1$, as expected for a minimum uncertainty state (Wehrl 1978).

As an example, Figs. 2 and 3 show the time evolution of the Husimi distribution of a minimum uncertainty wavepacket with $s_0 = s_1 = 1$ and $s_0 = s_1 = 2$ moving in a harmonic potential with unit mass and frequency. In Fig. 2, the wavefunction is a coherent state of the harmonic oscillator and moves without changing its form. In Fig. 3, we have a squeezed oscillator state, which changes its form and uncertainty product as monitored by the entropy S.

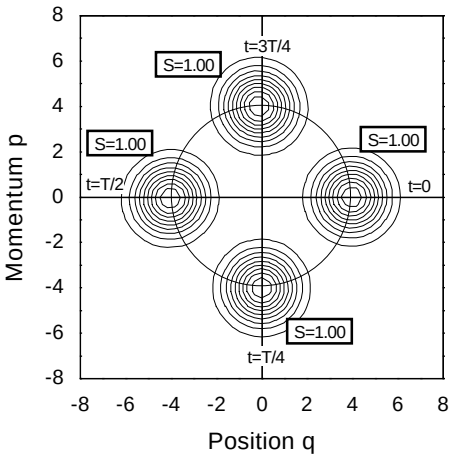

Fig. 2. Contour plot of the Husimi distribution (squeezing parameter $s_1 = 1$) for an initial minimum uncertainty wavepacket ($s_0 = 1$) moving in a harmonic oscillator with unit mass and frequency.

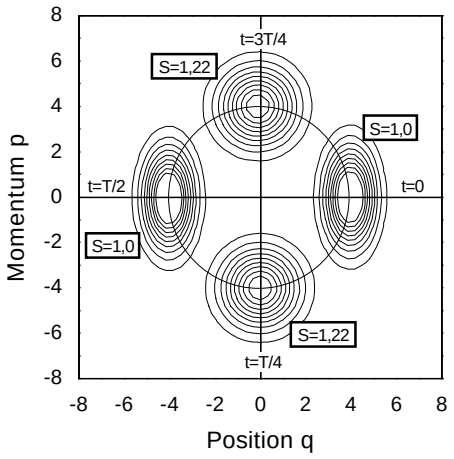

Fig. 3. Contour plot of the Husimi distribution (squeezing parameter $s_1 = 2$) for an initial minimum uncertainty wavepacket ($s_0 = 2$) moving in a harmonic oscillator with unit mass and frequency.

4 Case Study: A Driven Anharmonic Quantum Oscillator

Various paradigmatic systems are investigated repeatedly in the literature to explore the properties of quantum systems, which are classically chaotic. Here we study the time evolution of a wavepacket for a forced quartic oscillator

$$H(p, q, t) = \frac{p^2}{2m} + bq^4 - fq\cos(\omega t) \ , \tag{17}$$

which is time-periodic with period $T = 2\pi/\omega$. We choose parameter values $b = 0.25$, $f = 0.5$ and $\omega = 1$, a case for which the classical – quantum correspondence (Ben-Tal et al. 1992, 1993) and the semiclassical EBK quantization of regular quasienergy states (Bensch et al. 1992), (Thylwe and Bensch 1994a, 1994b) has been investigated recently (see also Mirbach and Korsch (1994), where different parameters are chosen).

4.1 Classical Phase Space Dynamics

The classical dynamics for this system is typical and shows a mixed regular and chaotic behavior depending on the initial conditions. Solving the classical equations of motion

$$\frac{\mathrm{d}p}{\mathrm{d}t} = -\frac{\partial H}{\partial q} = -4bq^3 + f\cos(\omega t) \quad , \quad \frac{\mathrm{d}q}{\mathrm{d}t} = \frac{\partial H}{\partial p} = \frac{p}{m} \tag{18}$$

for a specified initial condition $(p(0), q(0)) = (p_0, q_0)$ one obtains the phase space trajectory $(p(t), q(t))$. Figure 1 shows a stroboscopic plot of the trajectory at times $t_n = nT$, $n = 0, 1, 2, \ldots$, for selected initial conditions. There is a clear division of phase space into three different regions: A chaotic region generated by a single trajectory is sharply separated from an outer regular region. A second regular region is centered on a T-periodic trajectory and appears as a regular island embedded in a chaotic sea. By closer inspection, one observes additional smaller chains of stability islands close to the boundary between the inner island and the chaotic sea. The phase space area of the inner island is 2.25 and the chaotic sea covers an area of 7.85.

For different choices of the parameters, the overall appearance (a chaotic sea bounded by an outer regular region) is the same. The detailed structure of the inner stability islands changes, however, and shows characteristic bifurcations. The case studied here is selected because of its structural simplicity.

4.2 Quantum phase Space Dynamics

A minimum uncertainty wavepacket $\psi_{p_0,q_0}(x, 0)$ (see Eq. (12)) localized initially at a position (p_0, q_0) in phase space is propagated in time using a value $\hbar = 0.05$ (note that in the dimensionless units used here – by, e.g., setting the field frequency equal to unity – the Planck constant of the system depends on the parameters and can therefore be adjusted). At times $t_n = nT$, the Husimi density

$$\rho_{\mathrm{H}}(p, q; p_0, q_0; t_n) = \left| \int \phi^*_{p,q}(x)\psi_{p_0,q_0}(x, t_n)\mathrm{d}x \right|^2 \tag{19}$$

is computed on a grid of 50×50 points in (p, q) space. The grid covers the same region as the classical phase space shown in Fig. 1.

Let us first study the quantum phase space dynamics for a wavepacket localized at $(p_0, q_0) = (0, 0.6)$ initially, which is inside the classically chaotic region

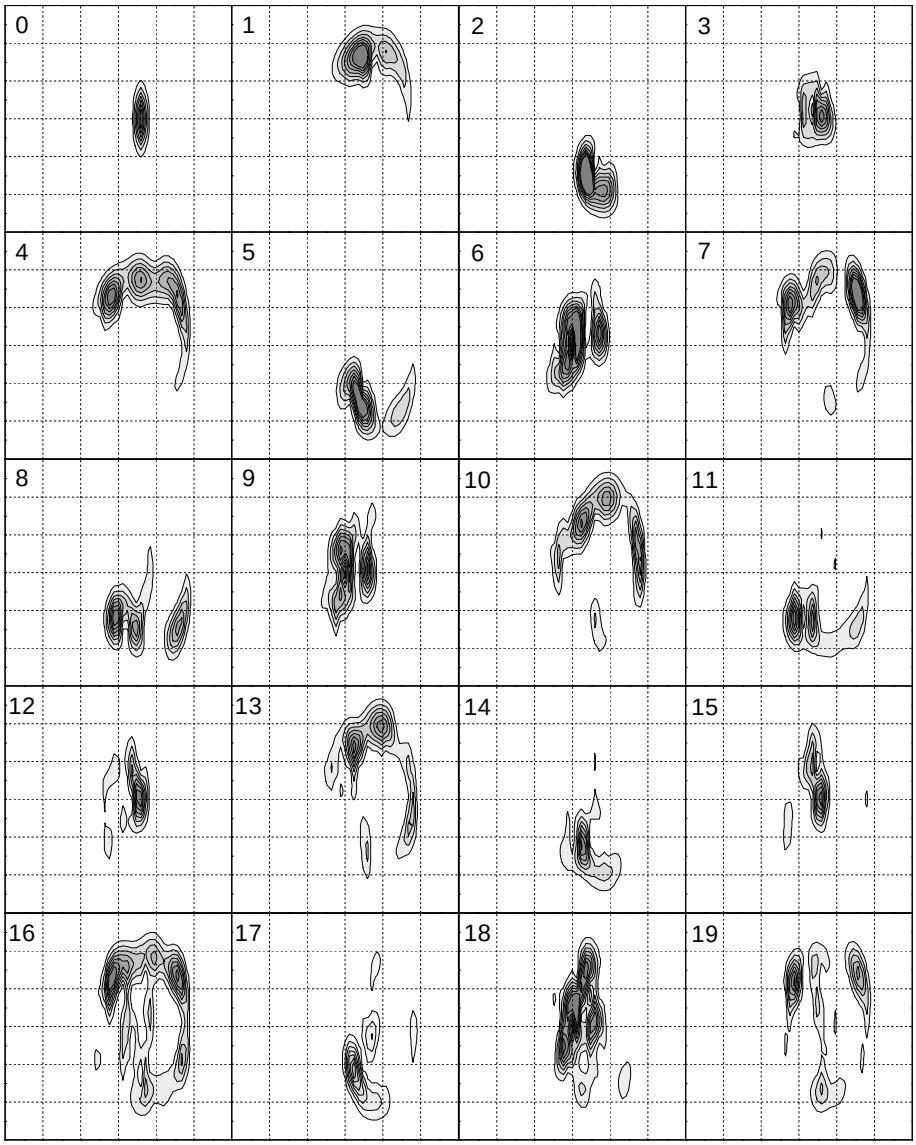

Fig. 4. Contour plots of the first 20 Husimi distributions at times $t_n = nT$. Shown is the region $[-3 : 3]$ with q on the horizontal and p on the vertical axis. Picture number 0 shows the initial minimum uncertainty state at $(p_0, q_0) = (0, 0.6)$ with squeezing parameter $s = 5$.

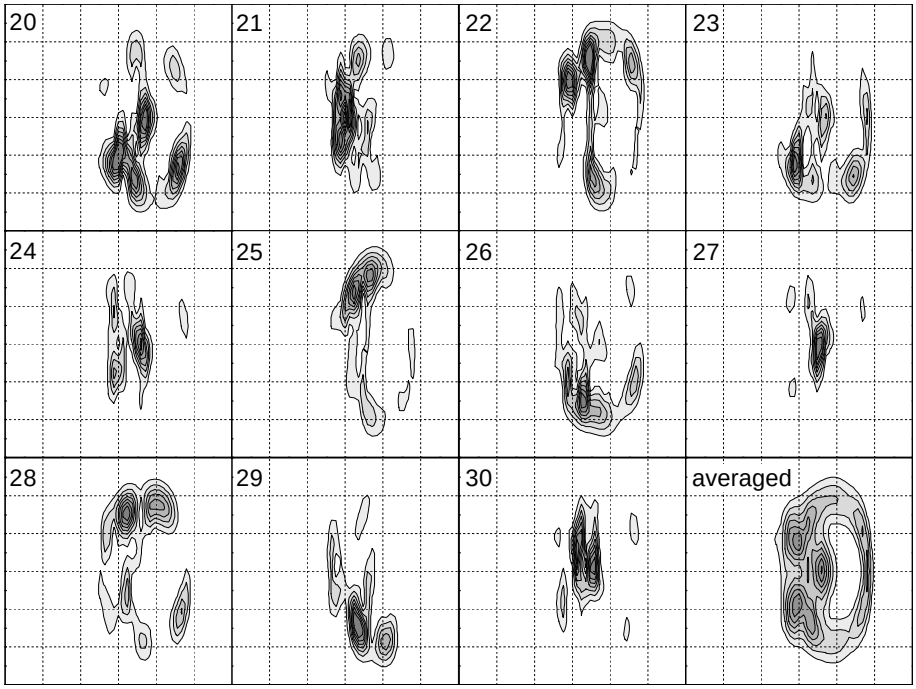

Fig. 5. Same as Fig. 4 for times t_n, $n = 20, \ldots, 30$. The last graph shows an average over periods 20-120.

(the squeezing parameter of $s = 5$ is adapted to a harmonic approximation to the center of the inner regular island). In the computation, the Goldberg algorithm (see Sect. 2) is used with mesh size $\varepsilon = 0.005$ and time-step $\delta = 0.001$. Figures 4 and 5 show the Husimi densities for the first 30 periods as contour plots. Dark regions mark large probabilities and correspond to strong localization of the wavefunction.

The first impression from Figs. 4 and 5 is an approximately periodic circulation of the center of the distribution with period $3T$. This can be checked quantitatively by computing the autocorrelation

$$C(t, t_0) = \int \psi^*(x, t_0)\psi(x, t)\mathrm{d}x \quad , \tag{20}$$

which measures the overlap of the wavefunction at time t with the initial distribution, and the recurrence probability

$$P_{\mathrm{R}}(t, t_0) = |C(t, t_0)|^2 \quad . \tag{21}$$

Figure 6 shows the recurrence probability for the first 50 periods. Up to $t = 20\,T$, one observes clear maxima at multiples of three. This periodicity is reflected in

the corresponding Fourier spectrum shown in Fig. 7. The strongest peak of the frequency spectrum appears at $\nu = 0.33/T$, which corresponds to period three. The same period-three circulation can be found if an initially Gaussian ensemble is propagated classically.

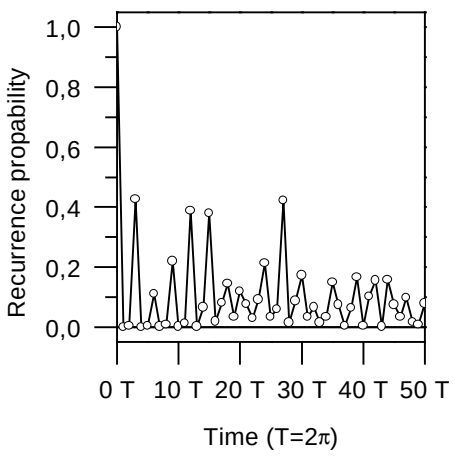

Fig. 6. Probability $C(t, t_0)$ for recurrence of the wavepacket to its initial position.

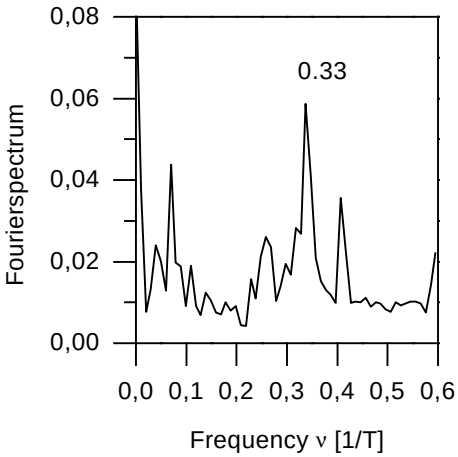

Fig. 7. Fourier spectrum of the recurrence probability shown in Fig. 6.

The increasing delocalization of the wavepacket can be measured quantitatively by means of the phase space entropy (15). Figure 8 shows the entropy

$$S_{p_0,q_0}(t_n) = -\frac{1}{2\pi\hbar} \int \rho_{\mathrm{H}}(p, q; p_0, q_0; t_n) \, \ln \rho_{\mathrm{H}}(p, q; p_0, q_0; t_n) \, \mathrm{d}p \, \mathrm{d}q \tag{22}$$

for the first 120 periods. Starting from the value of 1 for the initial minimum uncertainty state at time zero, the entropy increases within the first 20 periods, then it flattens into a plateau. For long times, the entropy fluctuates almost erratically with an average value of about $\overline{S} = 3.1$, which is somewhat below the value of $S_{\mathrm{cl}} = \ln(A/2\pi\hbar) \approx 3.2$ obtained from the classical chaotic phase space area $A = 7.85$. The entropy difference is due to the fluctuation of the quantum dynamics in contrast to the classical one, which approaches a uniform limiting distribution (see also the more detailed analysis for a driven rotor system (Moiseyev et al. 1994) based on the random vector model).

One can also study the long time average of the Husimi distributions

$$\bar{\rho}_{\mathrm{H}}(p, q; p_0, q_0) = \lim_{N \to \infty} \frac{1}{N - N_0 + 1} \sum_{n=N_0}^{N} \rho_{\mathrm{H}}(p, q; p_0, q_0; t_n) \tag{23}$$

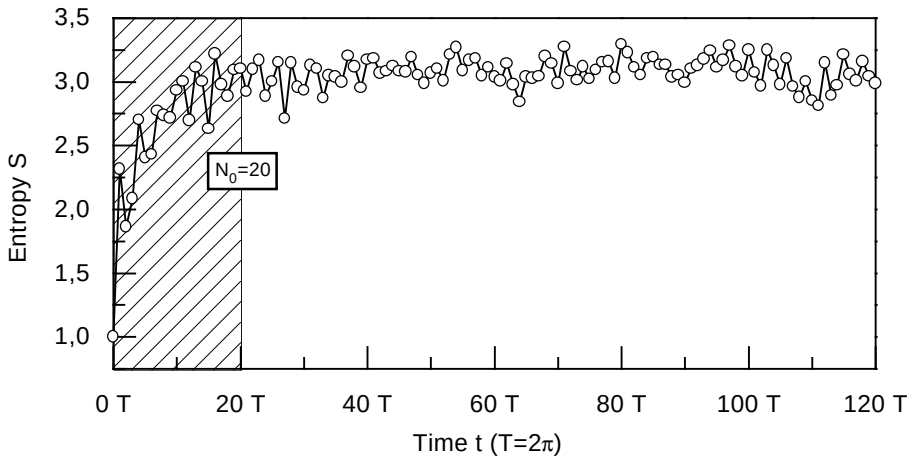

Fig. 8. Time dependence of the phase space entropy for the distributions shown in Figs. 6 and 7.

(in numerical computations using a finite value of N, the first N_0 distributions during the initial delocalization should be neglected to improve the convergence).

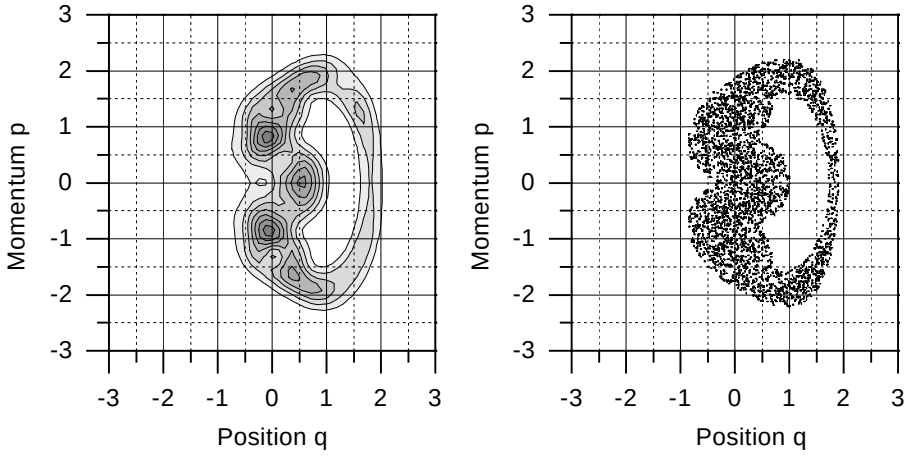

Fig. 9. Contour plot of a time-averaged quantum Husimi distribution for wavepacket (c) and classical Poincaré section for a chaotic trajectory.

Figure 10 shows three time-averaged Husimi distributions for different initial

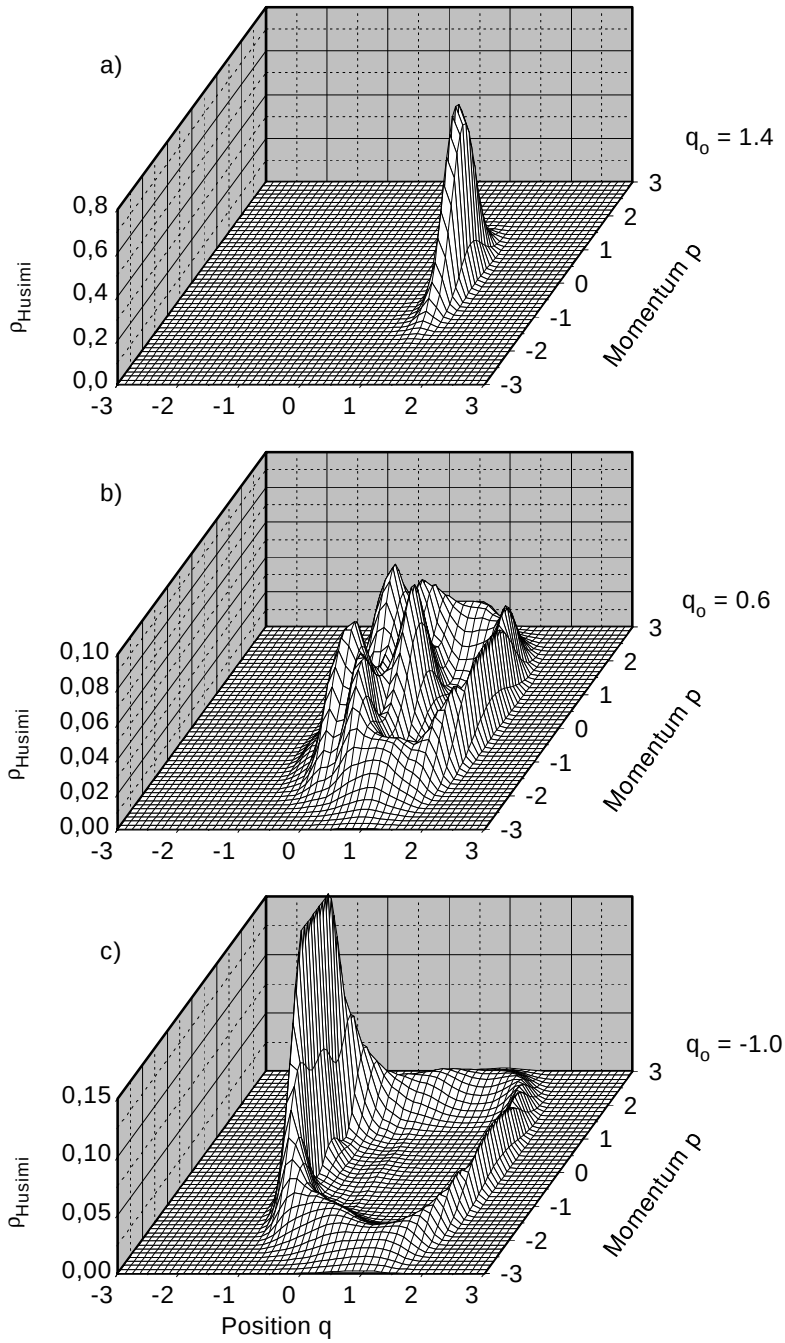

Fig. 10. Time averaged Husimi distributions of a minimum uncertainty wavepacket located initially at ψ_{p_0,q_0} with $p_0 = 0$ and (a) $q_0 = 1.4$ (at the center of the stability island), (b) $q_0 = 0.6$ (in the chaotic region), and (c) $q_0 = -1.0$ (in the outer regular region).

distributions centered at ψ_{p_0,q_0} with $p_0 = 0$ and (a) $q_0 = 1.4$ (at the center of the stability island), (b) $q_0 = 0.6$ (in the chaotic region), and (c) $q_0 = -1.0$ (in the outer regular region). The wavefunction has been propagated over $N = 101$ periods; the first $N_0 = 20$ periods are not included in the average.

The time-averaged distributions can be compared with the classical Poincaré section in Fig. 1. We observe a clear correspondence with classical phase space dynamics in the three regions. In case (a) the distribution remains localized on the stability island. In case (b) the distribution spreads out over the classically chaotic region, showing, however, an additional quantum localization in three regions of phase space (see Fig. 9), which is a quantum interference phenomenon. On the other hand, the strong concentration on the region close to $(0, -1)$ in case (c) is a classical effect (Bensch et al. 1992), which is also reproduced by propagation of classical phase space densities.

4.3 Quasienergy Spectra

The time evolution of a wavepacket provides also information about the spectrum of the system, which can be computed from the autocorrelation function (20). In the present case of time-periodic Hamiltonians $H(t+T) = H(t)$, this is the spectrum of the quasienergies ϵ_α defined by the quasienergy states (or Floquet states)

$$\psi_\alpha(t) = e^{-\mathrm{i}\epsilon_\alpha t/\hbar} u_\alpha(t) \ , \tag{24}$$

where the u_α are T-periodic. This definition determines the quasienergies only up to integer multiples of $\hbar\omega = h/T$. Often it is therefore convenient to introduce the quasiangles $\theta_\alpha = \epsilon_\alpha T/\hbar$. Expanding the wavefunction in terms of the quasienergy states $\psi(t) = \sum_\alpha c_\alpha \psi_\alpha(t)$ with constant coefficients c_α, the Fourier transform of the autocorrelation

$$C_n = C(t_n, t_0) = \sum_\alpha |c_\alpha|^2 \mathrm{e}^{-\mathrm{i}\theta_\alpha n} \tag{25}$$

after n periods (compare Eq. (20)) yields

$$C(\theta) = \sum_n C_n \mathrm{e}^{\mathrm{i}\theta n} = 2\pi \sum_\alpha |c_\alpha|^2 \delta(\theta - \theta_\alpha) \ . \tag{26}$$

In praxis, the computation is not extended to infinity and for a finite cutoff at $n_{\max}$ a window function, e.g. $w_n = (1 - \cos(2\pi n/n_{\max}))/2$, must be introduced into the n-sum in Eq. (26), which reduces the spurious oscillations produced by the cutoff and smoothes the δ-functions into line shape functions $\mathcal{L}(\theta - \theta_\alpha)$, which are determined by the window function. In addition, the quasienergy function at time $t_0 = 0$ is given by

$$\psi_\alpha(0) \propto \sum_n^N \psi(t_n) w_n \mathrm{e}^{\mathrm{i}\theta_\alpha n} \ , \tag{27}$$

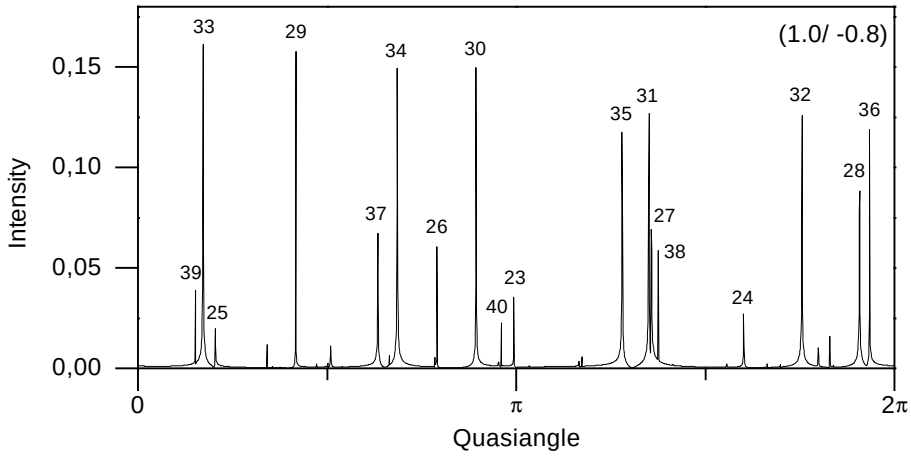

Fig. 11. Fourier transform of the autocorrelation function for a wavepacket placed initially at $(1, -0.8)$, which is inside the chaotic sea and close to the boundary to the outer regular region (see Fig. 1). The peaks appear at the quasiangles θ_α.

where the proportionality constant is obtained by normalization. As an example, Fig. 11 shows the Fourier transform of the autocorrelation function for a wavepacket initially placed at $(1, -0.8)$, i.e. inside the chaotic region of Fig. 1. The peaks appear at the quasiangles θ_α.

A subsequent analysis of the Husimi distributions of the corresponding quasienergy states ψ_α provides information about the localization properties on different regions in phase space. Furthermore, by computation of a sufficiently large number of quasienergies or quasiangles, the statistical properties of the quasienergy spectra can be tested. The prediction is, e.g., that the nearest neighbor distance follows a Poisson distribution for those states localizing on a regular region, whereas those corresponding to a chaotic regime are Wigner distributed (see, e.g., Haake (1992) and references therein).

4.4 Chaotic Tunneling

As an interesting application, one can investigate the influence of a time-periodic field on the dynamics of a wavepacket moving in a bistable potential, e.g. a double minimum potential. A system studied recently by various authors is the potential

$$V(q,t) = bq^4 - dq^2 + fq\cos(\omega t) \ , \tag{28}$$

a frictionless Duffing oscillator, with values $b = 0.5$, $d = 10$, $\omega = 6.07$, and $\hbar = 1$ for the parameters (Lin and Ballentine 1990, 1992).

For vanishing external driving field, we have a simple time-independent double well potential and the energy E is conserved. For energies below the barrier, a quantum wavepacket localized in the left potential well tunnels through the barrier – the classically inaccessible region in phase space – and appears on the right hand side. This process continues and we observe a tunneling oscillation between the two minima. This phenomenon is well understood and can be described semiclassically (see, e.g., Child (1991)) in terms of the action integral

$$\kappa = \int_{q_-}^{q_+} \sqrt{2m|E - V(q)|}\, \mathrm{d}q \quad , \tag{29}$$

over the barrier, where $q_\pm$ are the turning points. Well below the barrier, i.e. for large κ, the tunneling probability is $\mathrm{e}^{-2\kappa}$ and the tunneling splitting of the almost degenerate energy eigenvalues is given by

$$\Delta E \approx \frac{\hbar\overline{\omega}}{\pi}\, \mathrm{e}^{-\kappa} \quad , \tag{30}$$

where $\overline{\omega}$ is the classical frequency in a single well. A superposition of these states oscillates with period $T_{\mathrm{osc}} = 2\pi\hbar/\Delta E$ between the two wells.

When the field is switched on, the situation is much more complicated by the fact, that the classical motion is chaotic and there is no conserved quantity in the chaotic region between the wells, and hence no equivalent of the tunneling integral (29). Typically, the two potential minima turn into stability islands and the curve separating the single well motion from the double well oscillation at higher energies (the 'separatrix') is destroyed by the interaction with the field. Instead, a chaotic separatrix layer develops, which grows with increasing field strength.

Tunneling through such a chaotic layer is still far from being understood and the theory of such tunneling transitions is an active field of contemporary research (see, e.g., Peres (1991), Plata and Gomez Llorente (1992), Casati et al. (1994), or Grossmann et al. (1991a,b, c, 1993), Utermann et al. (1994) for studies of a driven double well oscillator and Grobe and Haake (1987), Casati et al. (1994), Averbuckh et al. (1995) for related studies of a kicked or driven rotor).

Figure 12 shows a stroboscopic Poincaré section of the system (28) for the parameters given above. Results from three classical trajectories are shown: One trajectory generates the chaotic sea, the other two are regular and move around the left or right island, respectively. Transitions between the left and the right island are classically forbidden. Quantum mechanically, such a transition is allowed, however.

On the right hand side of Fig. 12, a wavepacket started on the left island (more precisely a minimum uncertainty wavepacket (12) centered at $(p_0, q_0) = (0, -1.5)$ with $s = 1$) is shown after one period T of the driving field. It is obvious, that the distribution is beginning to populate the right stability island. After 58 periods, a considerable part of the distribution is found there, and after 115 periods almost the whole wavepacket has tunneled to the opposite island, as

demonstrated in Fig. 13. It is remarkable that the distribution localizes on the regular island again, despite of the fact, that it has tunneled through the region, where the classical dynamics is chaotic.

The recurrence probability (21) in Fig. 14 shows the continuation of the tunneling process with increasing time. We observe an overall oscillation with period

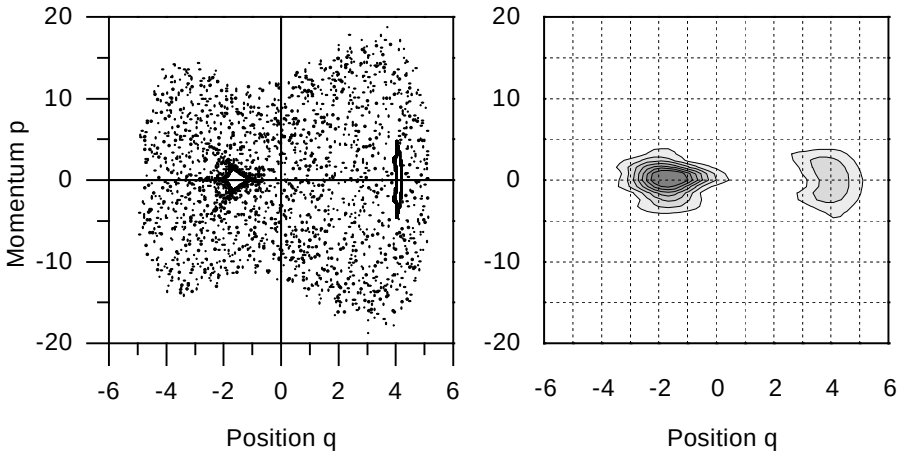

Fig. 12. Poincaré section of classical phase space (left) and quantum Husimi distribution (right) of a wavepacket started on the left island after one period.

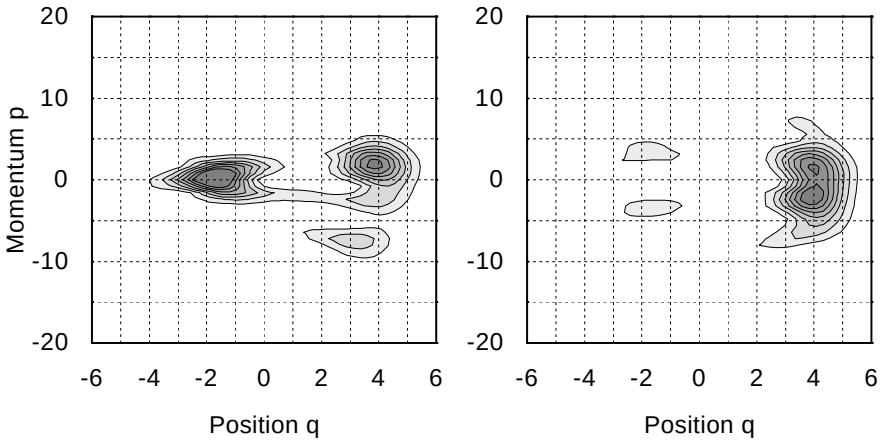

Fig. 13. Quantum Husimi distribution of a wavepacket started on the left island after 58 (left) and 115 (right) periods.

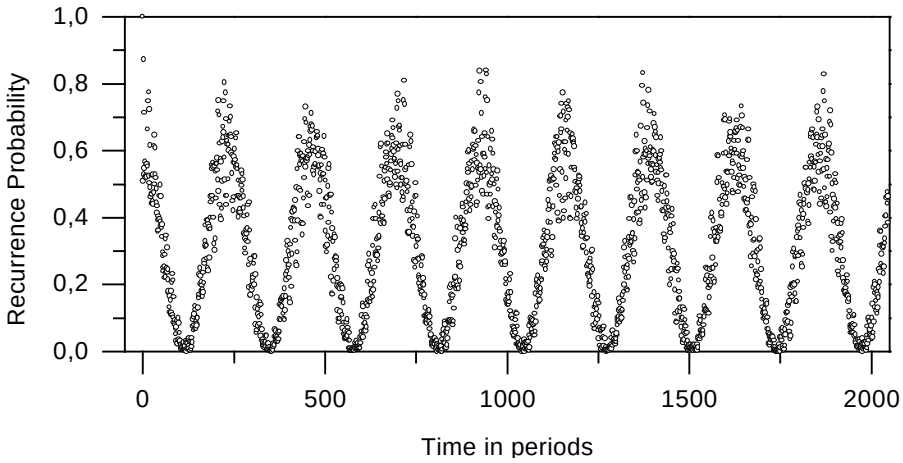

Fig. 14. Recurrence probability as a function of time.

$114\,T$ of a certain fraction of the distribution between the two islands. This *'coherent tunneling'* (Lin and Ballentine 1990, 1992) can be explained in terms of quasienergy (Floquet) states of different symmetry localizing on both islands (Grobe and Haake (1987), Peres (1991), Plata and Gomez Llorente (1992), Averbuckh et al. (1995). Their superposition leads to states oscillating between the islands with a period proportional to the inverse of the difference of the two quasienergies. This can be checked by computing the quasienergies and the Husimi distribution from the autocorrelation function as discussed in Sect. 4.4. The results are shown in Figs. 15 and 16.

Recent observations from numerical computations suggest, that the quasienergy splittings for chaotic tunneling do *not* follow the simple semiclassical law (30) when $\hbar$ is varied (Roncaglia et al. 1994). Instead, they show a seemingly irregular behavior.

5 Concluding Remarks

In this article we have tried to demonstrate some of the numerical techniques used to explore the manifestation of classical chaos in the corresponding quantum system. We have confined ourselves to the case of a driven anharmonic oscillator and presented some of the techniques using quantum dynamics in phase space. Let us finally give a brief description of a method suggested recently for developing a global picture of the phase space structure of a quantum system (Mirbach and Korsch 1995). The basic idea is to compute the long time average $\overline{S}(p_0, q_0)$ of quantum phase space entropy (22) for *all* initial positions (p_0, q_0) of the initial wavepacket. This function provides a quantitative measure of the phase space localization properties of the quantum system in analogy to the classical Poincaré

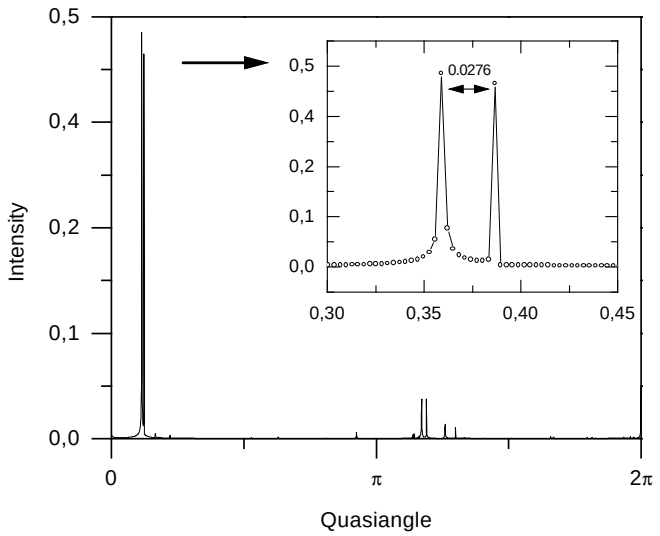

Fig. 15. Quasienergy spectrum of the autocorrelation function (see Fig. 14). The inset shows a magnification of the two strongest peaks.

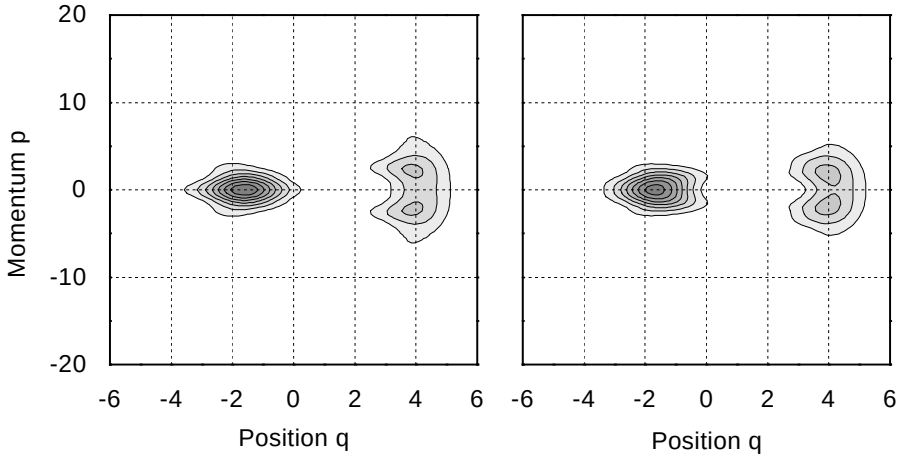

Fig. 16. Husimi distributions of the quasienergy doublet shown in Fig. 15.

section. Numerical studies for a driven rotor system (Moiseyev et al. 1994) have been reported recently (Mirbach and Korsch 1995) and the (semiclassical?) explanation of this phenomenon is not yet clear.

References

Averbuckh, V., Moiseyev, N., Mirbach, B., and Korsch, H. J. (1995): Z. Phys. D, in press

Becker, J., Ernesti, A., and Korsch, H. J. (1996): in preparation

Becker, J., Speckert, F., Korsch, H. J., and Jodl, H.-J. (1988): Phys. u. Didaktik **16** 127

Bensch, F., Korsch, H. J., Mirbach, B., and Ben-Tal, N. (1992): J. Phys. A **25** 6761

Ben-Tal, N., Moiseyev, N., and Korsch, H. J. (1992): Phys. Rev. A **46** 1669

Ben-Tal, N., Moiseyev, N., Fishman, S., Bensch, F., and Korsch, H. J. (1993): Phys. Rev. E **47** 1646

Casati, G., Graham, R., Guarneri, I., and Izrailev, F. M. (1994): Phys. Lett. A **190** 159

Casati, G., Guarneri, I., and Smilansky, U., Eds., (1993): *Quantum Chaos*, Intern. School of Physics Enrico Fermi, Como 1991 (North-Holland, Amsterdam)

Casati, G., and Molinari, L. (1989): Prog. Theor. Phys. Suppl. **98** 287

Child, M. S. (1991): *Semiclassical mechanics with molecular applications* (University Press, Oxford)

Cvitanović, P., Percival, I., and Wirzba, A., Eds., (1992): *Quantum Chaos – Quantum Measurement*, NATO ASI Copenhagen 1991 (Kluver, Dordrecht)

De Raedt, H., and Michielsen, K. (1994): Computers in Physics **8** 600

Feit, M. D., Fleck Jr., J. A., and Steiger, A. (1982): J. Comput. Phys. **47** 412

Feng, D. H., and Yuan, Y.-M. (1992): *Quantum Non-Integrability* (World Scientific, Singapore)

Gay, J.-C. (1992): *Irregular Atomic Systems and Quantum Chaos* (Gordon and Breach, Montreux)

Goldberg, A., Schey, H. M., and Schwarz, J. L. (1967): Am. J. Phys. **35** 177

Grobe, R., and Haake, F. (1987): Z. Phys. B **68** 503

Grossmann, F., Dittrich, T., and Hänggi, P. (1991c): Physica B **175** 293

Grossmann, F., Dittrich, T., Jung, P., and Hänggi, P. (1993): J. Stat. Phys. **70** 229

Grossmann, F. Jung, P., Dittrich, T. and Hänggi, P. (1991a): Phys. Rev. Lett. **67** 516; (1991b): Z. Phys. B **84** 315

Gutzwiller, M. C. (1990): *Chaos in Classical and Quantum Mechanics* (Springer, New York)

Gutzwiller, M. C. (1992): Scientific American, Jan. 1992, 26

Haake, F. (1992): *Quantum Signatures of Chaos* (Springer, Berlin, Heidelberg, New York)

Heller, E. J. and Tomsovic, S. (1993): Physics Today, 38

Husimi, K. (1940): Proc. Phys. Math. Soc. Japan **22** 264

Ikeda, K., Ed., (1994): *'Quantum Chaos'* Intern. Seminar *"Quantum and Chaos: How Incompatible?"*, Progr. Theoret. Phys. Suppl. **116** (special issue)

Koonin, S. (1986): *Computational Physics* (Benjamin–Cummings, Menlo Park)

Korsch, H. J. and Jodl, H.-J. (1994): *Chaos – A Program Collection for the PC* (Springer, Heidelberg, New York)

Leforestier, C., Bisseling, R. H., Cerjan, C., Feit, M. D., Friesner, R., Guldberg, A., Hammerich, A., Jolicard, G., Karrlein, W., Meyer, H.-D., Lipkin, N., Roncero, O., and Kosloff, R. (1991): J. Comput. Phys. **94** 59

Lin, W. A., and Ballentine, L. E. (1990): Phys. Rev. Lett. **65** 2927; (1992): Phys. Rev. A **45** 3637

Mirbach, B., and Korsch, H. J. (1994): J. Phys. A **27** 6579
Mirbach, B., and Korsch, H. J. (1995): Phys. Rev. Lett. **75** 362
Moiseyev, N., Korsch, H. J., and Mirbach, B. (1994): Z. Phys. D **29** 125
Nakamura, K. (1993): *Quantum Chaos: A new paradigm of nonlinear dynamics* (Cambridge University Press, Cambridge)
Ozorio de Almeida, M. (1988) *Hamiltonian Systems – Chaos and Quantization* (University Press, Cambridge)
Peres, A. (1991): Phys. Rev. Lett. **67** 158
Peskin, U., and Moiseyev, N. (1993): J. Chem. Phys. **99** 4590
Plata, J., and Gomez Llorente, J. M. (1992): J. Phys. A **25** L303
Press, W. H., Teukolsky, S. A., Vetterling, W. T., and Flannery, B. P. (1986): *Numerical Recipes* (Cambridge University Press, Cambridge)
Reichl, L. E. (1992) *The Transition to Chaos* (Springer, New York)
Roncaglia, R., Bonci, L., Izrailev, F. M. , West, B. J. , and Grigolini, P. (1994): Phys. Rev. Lett. **73** 802
Schneider, J. (1987): *Subbarrierenfusion als Tunneln von mehrdimensionalen Wellenpaketen.* (Thesis, Univ. München)
Schneider, J., and Wolter, H. H. (1988): In: Signorini, C., Skorka, S., Spolaore, P., and Vitturi, A., Eds.: *Heavy Ion Interactions around the Coulomb Barrier*, Springer Lecture Notes in Physics, Vol.317; (1991): Z. Phys. A **339** 177
M. Tabor, M. (1989): *Chaos and Integrability in Nonlinear Dynamics* (John Wiley, New York)
Takahashi, K. (1989): Prog. Theor. Phys. Suppl. **98** 109
Thylwe, K.-E., and Bensch, F. (1994): J. Phys. B **27** 5673
Thylwe, K.-E., and Bensch, F. (1994): J. Phys. B **27** 7475
Utermann, R., Dittrich, T., and Hänggi, P. (1994): Phys. Rev. E **49** 273
Visscher, P. B. (1991): Computers in Physics **5** 596
Wehrl, A. (1978): Rev. Mod. Phys. **50** 221